ceramics

MDPI

Review

Ceramics—The Forgotten but Essential Ingredients for a Circular Economy on the Moon

Alex Ellery

Department of Mechanical & Aerospace Engineering, Carleton University, Ottawa, ON K1S 5B6, Canada; aellery@mae.carleton.ca; Tel.: +1-613-261-3765

Abstract

Settlement on the Moon will require full exploitation of its resources if such settlements are to be permanent. Such in situ resource utilisation (ISRU) has primarily been focused on accessing water ice at the lunar poles and the use of raw lunar regolith as a compressive building material. Some work has also examined the extraction of metals, but there has been little consideration of the many useful ceramics that can be extracted from the Moon and how they may be fabricated. We introduce a strategy for full lunar industrialisation based on a circular lunar industrial ecology and examine the contribution of ceramics. We review ceramic fabrication methods but focus primarily on 3D printing approaches. The popular direct ink writing method is less suitable for the Moon and other methods require polymers which are scarce on the Moon. This turns out to be crucial, suggesting that full industrialisation of the Moon cannot be completed until the problem of ceramic fabrication is resolved, most likely in conjunction with polymer synthesis from potential carbon sources.

Keywords: ceramics; in situ resource utilisation; lunar industrialisation; lunar industrial ecology; ceramic 3D printing

Academic Editors: Francesco Baino, Pardeep Gianchandani, Enrico Fabrizio, Bartolomeo Megna and Manuela Ceraulo

Received: 31 May 2025
Revised: 12 August 2025
Accepted: 20 August 2025
Published: 22 August 2025

Citation: Ellery, A. Ceramics—The Forgotten but Essential Ingredients for a Circular Economy on the Moon. *Ceramics* **2025**, *8*, 107. https://doi.org/10.3390/ceramics8030107

1. Introduction

It is anticipated that human exploration of the Moon will evolve toward settlement on the Moon and that such settlement will require the exploitation of local lunar resources: in situ resource utilisation (ISRU). Most interest has been focussed on water ice mining in permanently shadowed craters at the South Pole, supplemented by the use of local regolith as a construction material. Regolith is a potential resource that may be 3D printed for the construction of lunar or Martian bases [1]. D-shaping and contour crafting are two of several methods that involve 3D printing regolith with binders or cements for constructing protective shells for such bases [2]. Both D-shaping and contour crafting require bulk volumes of binder imported from Earth. D-shaping utilises $MgCl_2$ binder to react with MgO in lunar regolith (Sorel cement), while contour crafting requires polymer binder. An example of a potentially in situ-resourced cement is sulpho-aluminate cement [3]. These approaches assume minimum processing of the resource to render it useful. A lunar base also requires internal infrastructure that may also be in situ-resourced [4]. Similarly, providing both electrical power and storage may be enabled using in situ resources [5,6]. Given the necessity for supporting human life within lunar bases, lunar water resources will be essential for hydroponic food growth [7]. Although regolith is a 3D printable ceramic in situ resource, we shall not address lunar base construction here, for which there are notably excellent reviews [8].

We are interested in building a lunar infrastructure from lunar resources to minimise the capital cost of launching infrastructure from Earth. This requires significant processing of lunar resources to yield functional materials. We concern ourselves with a specific approach to ISRU that yields a range of lunar mineral-derived materials, including ceramics that have high utility rather than native lunar regolith. Most efforts have been focussed on the extraction of metals from lunar minerals, but we shall consider the neglected ceramic resources on the Moon. It is expected that partial gravity on the Moon will have a negligible effect on processing methods compared with microgravity in orbit [9] or milligravity conditions associated with asteroid processing [10]. Nevertheless, the Moon imposes particular challenges due to its limited diversity of material resources, and this will dominate the feasibility of manufacturing ceramics.

We explore the manufacture and exploitation of ceramics derived from lunar resources. Section 2 briefly describes the Moon's mineralogy and volatiles to provide context to the subsequent sections. Section 3 defines the lunar industrial ecology as the context for exploring ceramics manufacture; Section 4 explores thermal sintering and the problem of brittleness; Section 5 explores ceramic 3D printing methods for the Moon and finds them wanting; Section 6 introduces the importance of polymers; Section 7 explores the use of clays; Section 8 briefly looks at non-clay lunar mineral uses; Section 9 discusses the use of direct thermal heating of ceramics using solar concentrators; and Section 10 concludes that polymers are an essential partner to ceramics and lunar industrialisation will flounder until an alternative to polymers can be found.

2. Lunar Resources

The Moon is covered in a layer of regolith with up to 20% glasses derived from fragmented parental rock with an average grain size of ~60–80 μm to a depth of ~4–5 m in the mare and ~10–15 m in the highlands [11]. Lunar mineralogy is broadly divisible into the anorthositic highlands and the basaltic mare. Anorthosite is dominated by the feldspar anorthite ($CaAl_2Si_2O_8$) while mare basalt may have high-Ti or low-Ti content, the former characterised by 10–20% ilmenite ($FeTiO_3$). The dominant minerals on the Moon are plagioclase feldspar (dominantly anorthite), pyroxene (such as augite $(Ca,Fe,Mg,Ti,Al)_2Si_2O_6$), olivine (dominated by forsterite Mg_2SiO_4), ilmenite and spinel (dominated by $MgAl_2O_4$) [12], all of which may be exploited as resources [13]. Orthopyroxene, olivine and spinel lithologies are located primarily on the lunar farside and are believed to have originated from large magmatic intrusions (plutons) from the mantle into the lunar crust [14]. Lunar minerals are highly oxidised, representing sources of oxygen through chemical or electrolytic reduction. However, the Moon is depleted in Na, Zn and Cu which imposes the necessity for lunar-constrained industrialisation. Halogens such as Cl and F are highly rarified but are concentrated in rare apatite ($Ca_5(PO_4)_3(OH,F,Cl)$) minerals.

KREEP basalts of the Procellarum KREEP Terrane on the northwest nearside are characterised by more Na-rich plagioclases and relatively elevated concentrations of potassium, rare earth elements (REE), phosphorus, thorium and uranium. The rare earth elements occur primarily in the form of ~μm monazite ($(Ce,La,Nd,Th)PO_4$) inclusions in pyroxene grains. The scarcer yttrobetafite ($(Ca,Y,U,Th,Pb,REE)_2(Ti,Nb)_2O_2$) is a potential source of yttrium, but this requires a complex series of chemical processes and reagents. Granite in (KREEPy) highland rocks is rare on the Moon, but it is a potentially useful resource for [15]: (i) silica minerals (primarily cristobalite rather than quartz); (ii) potassium feldspar $KAlSi_3O_8$; and (iii) zircons $ZrSiO_4$. However, the global abundance of granites is low. Indigenous lunar minerals are supplemented by minor amounts: <0.1% of meteoritic material from asteroid impacts including Fe, Ni, Co and troilite FeS.

Much more rarified is the lunar inventory of volatiles [16]. In particular, C, N and S are scarce within concentrations of ~1–100 ppm in regolith implanted by solar wind, though there are apparent higher concentrations in permanently shadowed craters such as Cabeus: 0.3% NH_3, 0.1% CO_2 and 0.04% CH_4. Similarly, water ice is concentrated in permanently shadowed craters of the lunar poles with concentrations of 5.6 ± 2.9% in the Cabeus crater. The cryogenic temperatures of ~25–40 K in permanently shadowed craters present major challenges for lunar operations. Concentration of ^{3}He is highly rarified ~20 ppb in mature ilmenite minerals. Although these volatiles may be released by heating ~700 °C, they are too scarce to be a viable resource. Carbon, in particular, averages ~100–120 ppm by weight of regolith so there is ~100 mg carbon per kg of regolith, i.e., extraction of 1 kg carbon would require excavating and heating 10 tonnes of regolith.

Nevertheless, the desirability for in situ resource utilisation is clear—it costs ~$750,000/kg to reach the surface of the Moon (Astrobotic Technology fees), so the use of in situ resources saves the transport cost, but it is essential that production machines' total lifetime mass throughput exceed its own mass. On Earth, this is higher at ~10^5 for excavation of bulk material than for manufacturing machines at ~10^3 which would be expected to be similar for the Moon, i.e., a saving of S750M–$75B per kg of landed lunar manufacturing asset.

The spinel $MgAl_2O_4$ is a resource available on the Moon that may be exploited directly (though contamination with ubiquitous Fe darkens glasses, so it may have to be synthesised from its constituents). Pure $MgAl_2O_4$ can also be synthesised, either from magnesia and alumina powders heated at 1800 °C, or from gibbsite ($Al(OH)_3$) in HCl solution and magnesia powders, heated to 80 °C for 7h, then precipitated when mixed with alkali hydroxide and then calcined at 1000–1400 °C [17], yielding optical properties tailored by the calcination temperature [18]. A common additive is 0.5% CaO which increases the sintering rate and yields maximum densification [19]. Sintering is typically achieved through hot isostatic pressing (HIP) [20]. The chief problem is its brittleness, which renders it difficult to machine, but laser-assisted and ultrasonic vibration-assisted machining of ceramics offer mitigation strategies [20]. $MgAl_2O_4$ has applications as refractory linings of high thermal resistance and low thermal expansion (with a melting point of 2135 °C), electric insulation, transparent optics from UV to IR (0.2–5.5 μm), immunity to chemical corrosion and impact-resistant armour of a very high hardness of 16 GPa. Transparent nanostructured $MgAl_2O_4$ ceramic with grain size of ~40 nm has a hardness of 31.7 GPa and Young's modulus 314 GPa under load that is twice that of large grained ~100–200 μm $MgAl_2O_4$ ceramics, consistent with the Hall–Petch relationship [21]. The addition of Y_2O_3 to $MgAl_2O_4$ grains tailors transparency to the infrared spectrum 0.2–0.6 μm [22]. As well as enhancing optical transparency, the addition of dopants enhances physical properties of strength and toughness by limiting grain boundary growth. The transparent $MgAl_2O_4$ ceramic exhibits enhanced fracture toughness when doped with 500 ppm of large ionic radii Ca and Y, where Y segregates around grain boundaries of Al and Ca segregate around grain boundaries around Mg [23]. High purity α-alumina may be doped with yttrium to segregate at grain boundaries to prevent grain growth and sintered at 1450 °C [24]. Similarly, yttrium-doping migrates to grain boundaries of transparent $ZnAl_2O_4$ ceramic, suppressing grain growth [25]. Ca is readily available from lunar anorthite but Y is more challenging to extract from lunar KREEP minerals requiring a suite of reagents. Rare earth element extraction from rare earth minerals requires dissolution in $(NH_4)_2SO_4$ electrolyte solution to beneficiate from the low-grade ore. Thence, treatment with ammonium bicarbonate ($CO_2 + NH_3 + H_2O \rightarrow (NH_4)HCO_3$) acts as a precipitant which is then burned to yield the rare earth elements. These reagents require N sources which would be imported from

Earth. These then must be separated under the constraint that they have similar physical and chemical properties.

3. Circular Lunar Industrial Ecology

A circular economy for terrestrial industry is premised on several properties that underlie the lunar industrial ecology: (i) maximum efficiency of mining, processing and production; (ii) recycling of waste to reduce pollution; and (iii) refurbishment and repair of products to extend their useful lifetime. Energy efficiency is sacrificed in favour of material closure through recycling or reuse. We have adopted the same philosophy for the lunar industrial ecology [13]. The guide for lunar resources is reflected in the Cheng'E-5 samples, suggesting bulk abundance of SiO_2 (44.9%), Al_2O_3 (17.5%), FeO (12.2%), CaO (12.1%), MgO (8.8%), TiO_2 (2.5%), Na_2O (0.44%), Cr_2O_3 (0.27%) and K_2O (0.11%) [26], though they do not occur in pure oxide form. We limited ourselves to extracting only metals that exceed 1% average concentration, though they exhibit higher concentrations in the commonest four lunar minerals: pyroxene, anorthite, orthoclase and ilmenite. Although there are only a handful of common rock-forming lunar minerals [27], they may be supplemented by iron–nickel asteroid material from impactors [28]. Our lunar industrial architecture emphasised industrial production capacity rather than lunar base infrastructure (Figure 1).

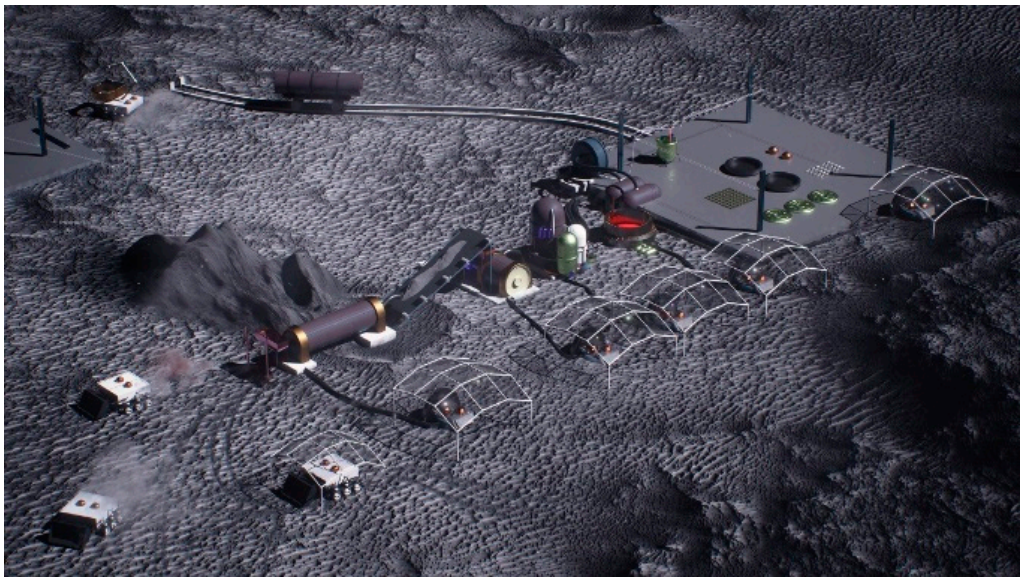

Figure 1. Lunar production architecture showing regolith acquisition by rover fleet, comminution, beneficiation, electrochemical processing and 3D printing facilities, supported by energy charging stations and transportation.

Our lunar industrial ecology was premised on such resources, and we restricted ourselves to building with lunar resources but permitted the import of reagents from Earth that are recycled but not consumed (Figure 2).

We can map the availability of processed lunar resources to the material functional requirements (demandite) of a spacecraft (Figure 3).

Lunar Ilmenite
$Fe^0 + H_2O \rightarrow$ ferrofluidic sealing
$FeTiO_3 + H_2 \rightarrow$ **TiO_2** $+ H_2O + Fe$
$2H_2O \rightarrow 2H_2 + O_2$
$2Fe + 1.5O_2 \rightarrow Fe_2O_3/Fe_2O_3.CoO$ - ferrite magnets
$3Fe_2O_3 + H_2 \leftrightarrow Fe_3O_4 + H_2O$) – formation of magnetite at 350-750°C/1-2 kbar
$4Fe_2O_3 + Fe \leftrightarrow 3Fe_3O_4$)

Nickel-Iron Meteorites
W inclusions → Thermionic cathodic material
Mond process:

Alloy	Ni	Co	Si	C	W

$W(CO)_6 \leftrightarrow 6CO + W$
$Fe(CO)_5 \leftrightarrow 5CO + Fe$ (175°C/100 bar) → Tool steel 2% 9-18%
$Ni(CO)_4 \leftrightarrow 4CO + Ni$ (55°C/1 bar) → Electrical steel 3%
$Co_2(CO)_8 \leftrightarrow 8CO + 2Co$ (150°C/35 bar) → Permalloy 80%
S catalyst Kovar 29% 17% 0.2% 0.01%
$4FeS + 7O_2 \rightarrow$ **$2Fe_2O_3$** $+ 4SO_2$
(Troilite) $SO_2 + H_2S \rightarrow 3S + H_2O$
$FeSe + Na_2CO_3 + 1.5O_2 \rightarrow$ **FeO** $+ Na_2SeO_3 + CO_2$ at 650°C
KNO_3 catalyst $Na_2SeO_3 + H_2SO_4 \rightarrow Na_2O + H_2SO_4 + Se \rightarrow$ photosensitive Se
↑_____|
$Na_2O + H_2O \rightarrow 2NaOH$
$NaOH + HCl \rightarrow NaCl + H_2O$

Lunar Orthoclase
$3KAlSi_3O_8 + 2HCl + 12H_2O \rightarrow KAl_3Si_3O_{10}(OH)_2 + 6H_4SiO_4 + 2KCl$
orthoclase illite silicic acid (soluble silica)
$2KAl_3Si_3O_{10}(OH)_2 + 2HCl + 3H_2O \rightarrow 3Al_2Si_2O_5(OH)_4 + 2KCl$
kaolinite
$[2KAlSi_3O_8 + 2HCl + 2H_2O \rightarrow Al_2Si_2O_5(OH)_4 + 2KCl +$ **SiO_2** $+ H_2O]$
$KCl + NaNO_3 \rightarrow NaCl + KNO_3$
$2KCl + Na_2SO_4 \rightarrow 2NaCl + K_2SO_4$

Lunar Olivine
$Fe_2SiO_4 + 4\ HCl + 4H_2O \rightarrow 2FeCl_2 +$ **SiO_2** $+ 2H_2O$
fayalite
$Mg_2SiO_4 + 4HCl + 4H_2O \rightarrow 2MgCl_2 + 2H_4SiO_4$ → Sorel cement
forsterite $MgCl_2 + 2\ NaOH \rightarrow Mg(OH)_2 + 2NaCl$
$Mg(OH)_2 \rightarrow$ **MgO** $+ H_2O$ → Sorel cement
600-800°C

Lunar Anorthite
$CaAl_2Si_2O_8 + 4C \rightarrow CO +$ **CaO** $+$ **Al_2O_3** $+ 2Si$ at 1650°C → CaO cathode coatings
$CaO + H_2O \rightarrow Ca(OH)_2$
$Ca(OH)_2 + CO_2 \rightarrow CaCO_3 + H_2O$
$CaAl_2SiO_8 + 8HCl + 2H_2O \rightarrow CaCl_2 + 2AlCl_3.6H_2O +$ **SiO_2** → fused silica glass + FFC electrolyte
$AlCl_3.6H_2O \rightarrow Al(OH)_3 + 3HCl + H_2O$ at 100°C
↑_____|
$2Al(OH)_3 \rightarrow$ **Al_2O_3** $+ 3H_2O$ at 400°C → $2Al + Fe_2O_3 \rightarrow 2Fe + Al_2O_3$ (thermite)
AlNiCo hard magnets
Lunar Pyroxene Al solar sail
$Ca(Fe,Al)Si_2O_6 + HCl + H_2O \rightarrow Ca_{0.33}(Al)_2(Si_4O_{10})(OH)_2.nH_2O + H_4SiO_4 + CaCl_2 + Fe(OH)_3$
Augite montmorillonite silicic acid iron hydroxide

Lunar Volatiles
$CO + 0.5\ O_2 \rightarrow CO_2$
$CO_2 + 4H_2 \rightarrow CH_4 + 2H_2O$ at 300°C (Sabatier reaction)
Ni catalyst
850°C 250°C
$CH_4 + H_2O \rightarrow CO + 3H_2 \rightarrow CH_3OH$ 350°C
Ni catalyst Al_2O_3 $CH_3OH + HCl \rightarrow CH_3Cl + H_2O$ 370°C +nH_2O
Al_2O_3 $CH_3Cl + Si \rightarrow (CH_3)_2SiCl_2 \rightarrow ((CH_3)_2SiO)_n + 2nHCl$ → silicone plastics/oils
↑_____|
$N_2 + 3H_2 \rightarrow 2NH_3$ (Haber-Bosch process)
Fe on $CaO+SiO_2+Al_2O_3$
$4NH_3 + 5O_2 \rightarrow 4NO + 6H_2O$

Figure 2. *Cont.*

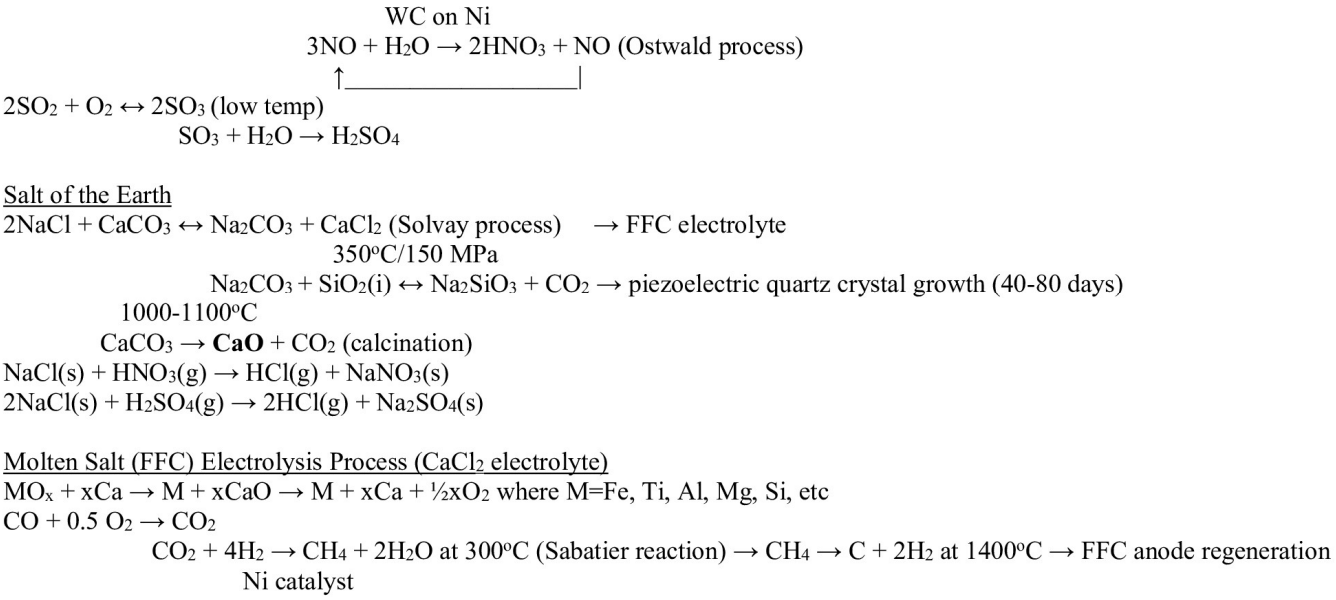

Figure 2. Lunar industrial ecology that converts raw lunar and asteroidal resources into final functional materials—inputs are on the left and applications are on the right (only a few feedback loops are shown).

Functionality (mass fraction)	Lunar-Derived Material
Tensile structures (25%)	Wrought iron Aluminium
Compressive structures (+50%)	Cast iron Regolith + binder
Elastic structures (trace)	Steel springs/flexures Silicone elastomers
Hard structures (3%)	Alumina
Thermal conductor straps (1%)	Fernico (e.g. kovar) Nickel Aluminum
Thermal radiators (3%)	Aluminium
Thermal insulation (3%)	Glass (SiO_2 fibre) Ceramics such as SiO_2
High thermal tolerance (4%)	Tungsten Alumina
Electrical conduction wire (7%)	Aluminium Fernico (e.g. kovar) Nickel
Electrical insulation (1%)	Glass fibre Ceramics (SiO_2, $Al_2O_3$and TiO_2) Silicone plastics Silicon steel for motors
Active electronics devices (vacuum tubes) (12%)	Kovar Nickel Tungsten Fused silica glass
Magnetic materials for actuators (5%)	Ferrite Silicon steel Permalloy
Sensory transducers (5%)	Resistance wire Quartz Selenium
Optical structures (11%)	Polished nickel/aluminium Fused silica glass lenses
Lubricants (trace)	Silicone oils Water
Power system (20%)	Fresnel lens + thermionic conversion Flywheels
Combustible fuels (+250%)	Oxygen Hydrogen

Figure 3. Lunar resources mapped to spacecraft functions—percentages refer to the proportion of a generic dry spacecraft, with excesses indicated for launch propellant to the Gateway and lunar habitat compressive structure.

We focussed primarily on the core of the lunar industrial ecology—the processing of the lunar highlands mineral anorthite. We adopted a geomimetic approach—geomimetics involves inspiration from the synthesis of natural materials through geological processes, such as hydrothermal vent processes at a high temperature and pressure [29]. We have

exploited a geomimetic technique inspired by geochemical weathering by weak carbonic acid, such as the dissolution of plagioclase feldspar into kaolinite and calcite [30]:

$$CaAl_2Si_2O_8 + H_2CO_3 + ½O_2 \rightarrow CaCO_3 + Al_2Si_2O_5(OH)_4$$

Kaolinite may be converted into gibbsite via hydrolysis:

$$Al_2Si_2O_5(OH)_4 + 5H_2O \rightarrow 2Al(OH)_3 + 2H_4SiO_4$$

From silicic acid, silica may be precipitated. We adopted HCl acid leaching on anorthite (and other lunar minerals) as our "artificial weathering". The first stage yielded calcium chloride and precipitated silica from silicic acid:

$$CaAl_2SiO_8 + 8HCl + 2H_2O \rightarrow CaCl_2 + 2AlCl_3{\cdot}6H_2O + 2SiO_2$$

Hydrous aluminium chloride decomposed into aluminium hydroxide at 100 °C with HCl partially recycled:

$$2AlCl_3{\cdot}6H_2O \rightarrow 2Al(OH)_3 + 6HCl + 9H_2O$$

Decomposition into alumina occurred at 400 °C:

$$2Al(OH)_3 \rightarrow Al_2O_3 + 3H_2O$$

We have demonstrated this process for the production of calcium chloride, alumina and silica from lunar highland simulant (LHS-1) that is dominantly anorthite [31], i.e., we have utilised 100% of the anorthite mineral. Calcium chloride is feedstock as $CaCl_2$ electrolyte for molten salt electrolysis [32]. Molten salt electrolysis requires much lower temperatures at 800–1000 °C than molten regolith electrolysis at 1650 °C. We have successfully demonstrated the reduction of alumina into 95% pure aluminium metal using molten salt electrolysis [33].

Our concern here is with the ceramics we have produced: alumina and silica. Alumina and silica are applied to situations where high wear resistance, high corrosion resistance, high electrical resistance and high thermal stability are required. We shall illustrate the potential of these two materials in more exotic applications. The float glass technique involves spreading a layer of molten glass onto a bed of molten metal. Fused silica or quartz glass SiO_2, although it has a high melting temperature, is chemically inert. The typical additives of Na_2CO_3 and $CaCO_3$ for sodalime glass, for reduced melting temperature and for hardening, respectively, or B_2O_3 for borosilicate glass of low thermal expansion, are not feasible on the Moon due to the paucity of Na and B but Al_2O_3 additives are feasible for aluminosilicate glass, for high heat tolerance. Glass may be strengthened to reduce its shatterability by heating to a high temperature and cooling it rapidly so the exterior cools faster than the interior. The temperature gradient ensures that the outer surface is in compression while the inner core is in tension (tempering). We do not consider electronics fabrication of Si semiconductors on the Moon to be feasible in the near-term [34]. There are other uses for silica. Silica aerogels may be manufactured from waterglass (sodium silicate) solution, which is acidified into silicic acid followed by gelation using a NH_4OH catalyst and then dried under special conditions [35]. They have multiple uses including high-performance thermal insulation.

It has been suggested that 20–25 m diameter heatshields of mass 40 tonnes for Earth re-entry at temperatures ~3000 °C may be fabricated on the Moon from sintered lunar silicates for the delivery of cargo [36]. Silica extracted from anorthite provides a superior material

for refractory heat shield tiles as used on the Space Shuttle. However, their adhesion was substandard. A 5:1 mixture of Al_2O_3:SiO_2 sintered at 1500 °C with a liquid aluminium dihydrogen phosphate ($Al(H_2PO_4)_3 \cdot xH_2O$) binder produces a high shear strength adhesive with a high temperature tolerance [37] that may be suitable. However, this is only feasible if we have access to phosphorus from KREEP (potassium rare earth elements phosphorus) basalt minerals on the Moon which are localised to the Procellarum region. We shall assume that this will be a possible scenario once lunar industrialisation has proceeded to maturity.

HCl "artificial weathering" is a general technique for yielding useful ceramics from lunar minerals. It may be applied to lunar forsterite to yield the ceramic, magnesia:

$$Mg_2SiO_4 + 4HCl + 4H_2O \rightarrow 2MgCl_2 + 2H_4SiO_4$$

$$MgCl_2 + 2\ NaOH \rightarrow Mg(OH)_2 + 2NaCl$$

$$Mg(OH)_2 \rightarrow MgO + H_2O$$

The mare mineral ilmenite may be reduced in the presence of hydrogen at 1000 °C to yield the ceramic rutile: $FeTiO_3 + H_2 \rightarrow Fe + TiO_2 + H_2O$. Typically, the molten Fe metal is tapped at 1600 °C (liquation) and the water is electrolysed to recycle hydrogen and recover oxygen, leaving rutile. HCl "artificial weathering" may also be applied to lunar orthoclase as a source of kaolinite clay ($Al_2Si_2O_5(OH)_4$) via illite clay ($KAl_3Si_3O_{10}(OH)_2$):

$$3KAlSi_3O_8 + 2HCl + 12H_2O \rightarrow KAl_3Si_3O_{10}(OH)_2 + 6H_4SiO_4 + 2KCl$$

$$2KAl_3Si_3O_{10}(OH)_2 + 2HCl + 3H_2O \rightarrow 3Al_2Si_2O_5(OH)_4 + 2KCl$$

Similarly, lunar pyroxene such as augite may be artificially weathered to yield montmorillonite clay:

$$Ca(Fe,Al)Si_2O_6 + HCl + H_2O \rightarrow Ca_{0.33}(Al)_2(Si_4O_{10})(OH)_2 \cdot nH_2O + H_4SiO_4 + CaCl_2 + Fe(OH)_3$$

In fact, acid weathering of pyroxenes at pH~3–4 proceeds more rapidly than that of feldspar, so basalt is enriched in feldspar on Mars [38]. Montmorillonite is an expanding clay, unlike illite and kaolinite, and is the primary ingredient in bentonite: (i) viscous agent in drilling mud; (ii) binder in sand casting—green sand is sand mixed with bentonite clay and water; (iii) absorbent (montmorillonite and kaolinite) in Fuller's earth as a cleaning agent; and (iv) feldspar and kaolinite may be supplemented by bentonite to form pottery. We shall focus on the processing of alumina, silica, magnesia and rutile and exploitation of clays as the ceramic resources available on the Moon. In doing so, we emphasise the multitude of useful properties these ceramics possess that make them so useful on the Moon as a complement to metals. Ceramics are often deployed in conjunction with metals. For example, lunar regolith simulant has been deployed for sand-casting and permanent mould-casting of metal parts such as aluminium [39]. Ceramics also have highly functional applications, e.g., Mg_2Si is a thermoelectric ceramic which can be manufactured from lunar resources. Ball-milled Mg_2Si fine-powder ~2–3 μm blended with an oxygen-free polymer (e.g., polyvinylidene difluoride) and dissolved in a dimethylformadine solution forms a thermoelectric paste which may be 3D printed into any shape and sintered at <400 °C limited by Mg_2Si thermal stability [40]. This requires the use of polymer.

4. Thermal Sintering of Lunar-Derived Ceramics

The most significant problem with the processing of ceramics is their hardness and brittleness at room temperature (an exception being Si_3N_4 which is plastic at room temperature under compressive loading [41]). Ceramics are typically formed through moulding,

casting and machining but 3D printing offers an alternative mode of manufacturing. Subtractive processing of ceramics is commonly accomplished through water jets pressurised to 300–600 MPa and laden with an abrasive such as alumina, which can implement cutting, drilling, shock peening and surface structuring. For constructive processing, dry ball milling is the approach for processing single ceramic powders or mixing powders for composites. Thermal sintering involves bonding of particles at ¼–¾ of the melting point. For ceramics, thermal sintering requires sintering temperature from 1000 to 2000 °C range. Reducing such temperatures to 1150 °C requires reducing particle sizes to ~10–100 nm by milling using grinding balls <1 mm in diameter and using additives such as <0.2% CaO and SiO_2 to inhibit grain growth [42]. Selective laser sintering/melting (SLS/M) cannot be employed for direct ceramic melting because of their high melting points, so a polymer, metal or glass binder of lower melting point is required to bind the ceramic particles. One of the chief challenges to direct thermal sintering is the thermal gradients introduced with generate cracks and brittleness. The chief advantage of direct thermal sintering on the Moon is that it requires no reagents and direct solar energy may be concentrated to high temperatures using Fresnel lenses [5].

To obviate high temperature >1000 °C ceramic processing, there are alternative approaches that may be exploited at a lower temperature, e.g., hydrothermal sintering at high pressure for densification, which requires aqueous solution [43]. Hot pressing under high temperature and pressure may be used to sinter particles into a 3D part with homogeneous microstructure. Artificial lithification is a hydrothermal press that compacts loose particles of anhydrous cement at 250 °C and 345 MPa with water into sedimentary rock [44]. Application to crystalline quartz or silica gel with aqueous NaOH solution to improve aqueous dissolution/precipitation reduces the required pressure to 20 MPa [45]. Hydrothermal hot pressing has been demonstrated for alumina, geopolymers, glasses, silica, titania and kaolinite clays. Subjection of nanosized alumina powder with silica gel to 4.5–5.0 GPa at room temperature yielded densified alumina and silica with a hardness of 5.7 GPa and 4.0 GPa, respectively [43]. Cold sintering involves lower applied pressures < 1 GPa and modestly elevated temperatures <350 °C by adding aqueous NaOH solution for lubrication of nanosized ceramic powders as a supersaturated solution, but this has yet to be demonstrated for alumina, silica or magnesia. Hence, hot hydrothermal synthesis under high pressure appears to be a viable approach to the densification of ceramics on the Moon.

One of the chief challenges to machining ceramics is their hardness and brittleness, so a major consideration is the introduction of durability to ceramics. Itacolumite sandstone is a highly flexible rock characterised by angular grain boundary microcracks that may be emulated by sintered aluminium titanate (Al_2TiO_5) powder [46]. Flexibility with flexural strength of 13 MPa is enhanced by a higher sintering temperature and sintering time with optimal values of 1550 °C and 12 h, respectively. Given the availability of TiO_2 on the Moon through hydrogen reduction of lunar ilmenite, this represents an unexplored material option for manufacturing aluminium titanate. Ceramic foams can utilise the superelasticity of alumina Al_2O_3 dispersed with 30% magnesia MgO, which suppresses grain growth of alumina [47]. Although the ductility of MgO-dispersed alumina is inferior to that of 3% yttria-stabilised zirconia, the former can be manufactured from lunar resources and expanded into dense shells. This is unexplored. Ceramic superplasticity occurs in some fine-grained ceramics (ZrO_2, Si_3N_4 and SiC) at a high temperature ~1500 °C through grain boundary sliding of intergranular glass phases [48]. This requires a grain size of <1 μm at a high temperature [49]. The application of an electric field can reduce the viscosity of such glass phases, making the ceramic more plastic [50]. Both these approaches of high temperature and applied electric fields are impractical. Borrowing dislocations in ceramics introduces metals with ceramic through sintering to permit dislocations at metal–ceramic

interfaces to enhance ceramic plasticity, e.g., Mo metal applied to La_2O_3 ceramic [51]. Sintered porous Si_3N_4 structures can be infiltrated by molten 6061 Al alloy under high pressure to enhance their fracture toughness [52]. Indeed, the addition of 10% Fe to lunar regolith simulant improved the density of thermally sintering blocks at 1035 °C by reducing cracks, yielding a compressive strength of 150 MPa and tensile strength of 20 MPa [53].

Ceramic matrix composites comprise a ceramic matrix impregnated with glass or metal fibres ~10^{-3} mm to impart non-brittleness. Alumina has high hardness, resistance to corrosion and wear and high thermal conductivity. Alumina particles may be employed as a reinforcement in aluminium metal composites, with optimal stress/strain properties of the composite favoured by small particle size of <10 μm and a higher sintering temperature at 600 °C over a 60 min sintering time [54]. An 80% alumina matrix with a uniform distribution of 20% nickel–iron superalloy steel particles may be fabricated using laser powder bed fusion at 1370 °C [55]. It exhibited porosity even after thermal sintering, due to poor adhesion between steel and alumina and insufficient melting of alumina. Polymer impregnation improved the compressive strength from 56 to 120 MPa. Similarly, digital light processing followed by spark plasma sintering at 1050 °C under 50 MPa pressure to remove a polymer binder has demonstrated the manufacture of fully dense functional grading of metal powder-regolith material [56]. A variation on UV-curable 3D printing involves 25–55% ZrO_2 nanoparticles dispersed in a UV-curable resin as a binder extruded into layers, subsequently cured using a UV laser, heated to 600 °C to remove the resin and sintered at 1450 °C [57]. NanoSiO_2 particle reinforcement may be incorporated into composites to extend their mechanical properties [58]. Bioinspired organic-inorganic materials offer high thermal stability with plastic mouldability, e.g., ceramic $CaCO_3$ with organic thioctic acid (TA) polymerised through S-S bonds, formed by adding $CaCO_3$ to an ethanol solution of TA [59]. Similarly, $CaCO_3$ nanoparticles may be crosslinked with polyacrylic acid to form a hydrogel which is stretchable, shapeable and self-healable [60]. Unfortunately, these materials require organic constituents.

5. Three-Dimensional Printing of Lunar-Derived Ceramics

Traditionally, ceramic parts are manufactured by the casting of slurries in moulds that are then cured and sintered, but such parts cannot assume complex geometries. Three-Dimensional printing of ceramics may be accomplished through fused deposition modelling (FDM), selective laser sintering (SLS), stereolithography (SLA), direct ink writing (DIW) and binder jetting [61]. FDM is an extrusion technique that prints from a ceramic powder-impregnated thermoplastic filament that is melted and extruded. The thermoplastic is typically PLA or ABS, but other higher performance polymers are possible, such as PEEK. PLA is notable because it can be derived from corn starch. Binder jetting is similar, in that powdered ceramic is sprayed with polymer but the binder is removed through polymer debonding at 280–650 °C, followed by thermal sintering at 1400–1500 °C [62]. Al_2O_3 is commonly printed with polymer and sintered in this way. A broad distribution of Al_2O_3 particle sizes yields higher densities and reduced shrinkage on sintering [63]. The use of such additives is common in FDM, but the quality of the parts printed is limited and unsuited to high performance applications such as high temperatures, as the matrix does not permit exploitation of the ceramics. Fibre-reinforced composites comprising high-elasticity fibres within a ceramic matrix such as alumina or silica compensate for brittleness in ceramics whilst retaining their high strength-to-weight ratio and resistance to corrosion and high temperature. Most commonly, the fibre material is SiC or graphite, but silica and alumina may be employed as fibres. Additive manufacturing of such composites favours the adoption of short fibres over continuous fibres, where 3D printing of the preformed composite is printed, followed by debinding and sintering [64]. As with ceramic 3D

printing, 3D printing may be through SLA, FDM, BJ, DIW or SLS. The adoption of ceramic fibres coated with nanophase iron permits the magnetic alignment of the fibres prior to SLA curing of polymer matrix composites (magnetic 3D printing) [65]. However, there remain challenges with poor bonding at fibre–matrix interfaces compared with traditional composite manufacturing.

Terrestrially, the most promising and versatile mode of 3D printing of ceramics is direct ink writing (DIW) or robocasting due to the wide range of inks [66]. DIW involves the extrusion of a non-Newtonian (shear-thinning) fluid polymer binder loaded with powder at a high density of >50%, such as a colloidal paste, to print 3D parts following sintering. The ink is designed with a yield stress described by the Herschel–Bulkley model: $\tau = \tau_\gamma + K\dot{\gamma}^n$ where τ = applied shear stress, τ_γ = yield stress, $\dot{\gamma}$ = shear rate, K = viscosity, n = degree of shear thinning (n = 1 for Newtonian fluids). During extrusion, shear-thinning is necessary, i.e., a decline in viscosity at higher shear rates to prevent clogging. Beyond τ_γ, shear thinning is described by a power law, $\tau = K\dot{\gamma}^n$. The 10–50 μm powder may be metal, polymer or ceramic but the binder is an organic polymer with additives. Typical polymers are much more complex than FDM polymers and include formaldehyde-phenol-urea, polycarboxylic acid, polyethylene glycol or polyvinyl acetate. For example, the hydrogel Pluronic F-127 comprises a 2:1 mix of polyethylene oxide and polypropylene oxide to provide both hydrophobic and hydrophilic properties. The paste must also include additives such as surfactants and dispersants to disperse the particles and prevent particle aggregation such as stearic acid [67]. After deposition, shape retention requires viscosity to increase as shear decreases. Thermal debinding at 200–600 °C removes the binder and must be slow to prevent crack formation, followed by thermal sintering at 1200–2000 °C, which generally yields 10–20% part shrinkage. Ceramic powder—silica, basalt, etc.—must be highly loaded into the slurry to reduce shrinkage after sintering. Ceramic powder comprises ~40–50% suspensions in the polymer fluid (inks) that are extruded as filaments flowing with decreased viscosity at increased shear [68]. The loading of solid powders imposes the need for larger nozzles than inkjet printing ~400–800 μm; this is because inkjet adopts low ceramic loading (<30%) in suspension for low-viscosity ink compared with high ceramic loading (<60%) for high-viscosity pastes for extrusion or SLA [69]. Inkjet printing is suited to ceramic nanoparticle suspensions in an ink characterised by an inverse Ohnesorge number of 1–10, but only simple structures can be printed in this way. Alumina is an ideal ceramic with high hardness, high compressive strength and resistance to both corrosion and wear that is also thermally and chemically stable at sintering temperatures. Ideal alumina loading is 53–56% with 2% Al metal to minimise shrinkage [70]. Sintering at 1550 °C yields ceramic parts of Al_2O_3 with 98% density. The addition of 3–7% carbon nanotubes imparts electrical conductivity to non-conducting alumina. A loading of 70% regolith simulant powder may be mixed with 30% polylactic-co-glycolic acid and other additives such as dichloromethane to form an ink that may be 3D printed into rubber-like structures with E = 1.8–13 MPa and 250% strain [71]. Although monomers glycolic acid and lactic acid are derivable from urine, the additives are not so readily manufactured from lunar resources. Multi-material 3D printing may be implemented by DIW through the extrusion of different inks with different functional properties [72]. The delivery of multiple composite inks may be through a single paste cartridge or multiple cartridges. Complex parts may be manufactured by DIW, such as gears, electrical components and sensors. Carbon nanotube or graphene in inks can form carbon networks in silicone elastomer matrices whose conductivity responds to pressure and/or temperature.

All these approaches to 3D printing ceramics and/or composites require the use of polymer binders which present major challenges for deployment on the Moon. However,

even if carbon sources can be found, the use of DIW is not feasible because it requires careful tailoring of inks which require an Earth-based infrastructure to realise.

6. Problem of Polymers

Carbon is scarce on the Moon, at ~120 ppm embedded in regolith by solar wind impregnation. There are other possible options. It is expected that concentrated asteroidal resources have been deposited into the Moon's surface by impacts [73,74]. A 1 km diameter carbonaceous chondrite striking the Moon at speeds $\leq$ 10 km/s and impact angles $\leq 15^{\circ}$ favour 85% survivability of C-rich (~10^9–10^{10} kg) and N-rich (~10^8–10^9 kg) solids ~20–30 km downrange of the impact site over a 60 km^2 area within <10 m of the surface [75]. Such impacts at <15° and <10 km/s by C-type asteroids are rare (~5 impacts in the last 3 By) but still yield greater C and N concentrations than solar wind impregnation of a typical permanently shadowed crater with ~6×10^5–6×10^8 kg C and N equally. Smaller impactors ~0.1 km would be more common ~500 delivering ~6×10^2–6×10^5 kg C and N equally for each impactor. They may present themselves through their phyllosilicate signature. The identification of graphite in Apollo 12 and Apollo 17 samples provides evidence of the survival of carbonaceous asteroid impacts favoured by porosity, obliquity and low velocity [76]. The Yutu-2 rover of Chang'e 4 has discovered a glassy material in a small 2 m diameter crater with a high 47% concentration of carbonaceous chondrite remnant from an impactor [77]. Even complex organic matter has been associated with pyroclastic beads recovered from Shorty crater by Apollo 17, derived from micrometeoritic kerogen [78]. So asteroid material may exist on the Moon but, if not, asteroids may be manoeuvred into lunar orbit and undergo a controlled descent to the lunar surface [79]. Once the asteroid has soft-landed on the Moon, it may be subject to processing under the Moon's gravity field. The latter scenario of asteroid manoeuvring is not technologically feasible in the near-term. Otherwise, the use of polymers requires its transport from Earth, which imposes a high transport burden. We examine two scenarios: (i) the recovery of diffuse solar-wind-implanted carbon volatiles so small quantities are available; and (ii) the discovery of an asteroid-delivered carbon source presenting copious amounts of carbon, permitting the manufacture of simple polymers.

In case (i), we have a restricted supply of carbon that must be husbanded and consumed frugally—one possibility is to synthesise polymers that use carbon only in its side chains but not its backbone. Inorganic silicone polymers are dominated by siloxanes with Si-O-Si backbones such as polydimethylsiloxane (PDMS), as well as related materials such as polysilazanes with Si–N–Si backbones. However, N is rarer than C on the Moon, ruling out the latter. Siloxanes (silicones) may be manufactured from syngas through the Rochow process via methanol [80]. Silicone can act as a binder for ceramic powders and a source of silica in the sintered ceramic part. Silicones have high temperature tolerance ~300 °C and high UV-resistance compared with C–C bond polymers. Preceramic polymers permit 3D printing of the polymer into complex parts, which is then converted into a ceramic through pyrolysis (ceramisation) at 600–1000 °C in an N_2 atmosphere which decomposes the organic component [81]. Silicone-based pre-ceramic polymer precursors can be 3D printed as extruded polymer and then cured into a SiOC ceramic by vacuum pyrolysis at 1100 °C after deposition. The printed SiOC has a compressive strength of 240 MPa. Pyrolysis in O_2 yields the formation of silicate ceramics by eliminating the carbon required for carbide formation. Silicones reduce the consumption of carbon but nevertheless do consume carbon, requiring recovery of CO/CO_2 during pyrolysis for recycling. Metallosiloxanes such as titanosiloxanes are silicones with metals in the polymer backbone Ti-O-Si, formed from TiO_2 at temperatures >900 °C [82]. They can act as zeolites. Aluminosiloxanes are inorganic polymers based on Al-Si-O backbone but are manufactured from complex precursors [83].

The aluminosiloxane Al(O'Pr),($OSiMe_3$) may be an organic precursor of $92Al_2O_3$-$8SiO_2$ ceramic [84]. However, complex precursors rule out aluminosiloxanes. Silicones and titanosilicones may be manufacturable in small quantities for specialist applications.

In case (ii), we can assume that a plentiful carbon source has been discovered and that we can synthesise simple plastics. The initial reactions for polymer synthesis from syngas to methanol are the same as for the Rochow process. We focus on synthesising transparent PMMA (polymethyl methacrylate) which has versatility of use, including as a tough acrylic glass, as a resist in electron beam lithography and, most relevant here, as transparent liquid MMA monomers that can act as UV photopolymers in SLA. Although manufacture of both PMMA and its photoinitiator require a source of N, we expect such to be available with C from carbonaceous chondrite deposits. Syngas may be converted to methanol using an alumina catalyst at 200–300 °C and 50–100 bar:

$$CO + 2H_2 \rightarrow CH_3OH$$

Methanol is converted to acetone through dehydrogenation:

$$2CH_3OH \rightarrow CH_3COCH_3 + H_2O + H_2$$

Acetone reacts with HCN to yield acetone cyanohydrin (ACH):

$$CH_3COCH_3 + HCN \rightarrow (CH_3)_2C(OH)CN$$

ACH is converted to transparent liquid MMA using H_2SO_4 at 80–120 °C:

$$(CH_3)_2C(OH)CN + CH_3OH + H_2SO_4 \rightarrow CH_2{=}C(CH_3)COOCH_3 + NH_4HSO_4$$

UV-initiated (benzoin initiator) polymerisation of MMA at 25–60 °C yields PMMA:

$$-[CH_2-C(CH_3)(COOCH_3)-]_n.$$

MMA monomer acts as a UV photopolymer by hardening into PMMA in the presence of the photoinitiator benzoin. Benzoin synthesis begins with conversion of methanol-to-benzene in the presence of a zeolite catalyst at 400–500 °C:

$$6CH_3OH \rightarrow C_6H_6 + 6H_2O$$

Zeolites are tetrahedral MO_4 units where M=Si or Al that act as selective catalysts. Benzene is converted to benzaldehyde through the Gattermann-Koch reaction using an $AlCl_3$ catalyst:

$$C_6H_6 + CO + HCl \rightarrow C_6H_5CHO$$

Benzoin condensation proceeds using an HCN catalyst:

$$2C_6H_5CHO \rightarrow C_6H_5CH(OH)COC_6H_5$$

Hence, we have the UV-photopolymer PMMA with its benzoin photoinitiator to permit the use of SLA. Refractory ceramic powder ~μm size such as silica or alumina may be dispersed at 50–65% by volume in a UV acrylate photopolymer (such as MMA) with photoinitiator (such as benzoin) and subjected to 150–200 μm layered stereolithography by UV laser [85]. The curing depth reachable by the UV laser is $d \propto \frac{1}{\Delta n^2}$ where n = refractive index difference between ceramic and solution derived from the Beer–Lambert law. The photopolymer binder is removed to reveal the ceramic part. Reduced gravity or micro-

gravity imposes criticality to the rheological properties of the ceramic slurry of 50% Al_2O_3 particles in a UV-curable glycol dimethylacrylate resin with a photoinitiator [86]. It behaves as a Bingham fluid in which low shear stress yields high solid-like viscosity, but there is a threshold shear stress that acts as a plastic yield stress. The viscoelasticity of the fluid is increased into a paste by 0.5% cellulose—cellulose is a single additive that can act as dispersant, plasticiser and coagulant that is derivable from vegetation. UV photopolymerisation builds the part layer-by-layer with a layer resolution of 50–100 µm. An 86% dense ceramic results after sintering at 1500 °C.

As we can see, the manufacture of polymers on the Moon would be a boon in opening up 3D printing techniques. Indeed, PMMA in particular exhibits high utility in opening SLA as a 3D printing technique. However, we cannot assume that these resources will be available so we must contend with a paucity of techniques for processing ceramics. The desirability for thermoplastic-type material properties for extrusion-based 3D printing has motivated interest in metallic glasses. Bulk metallic glasses such as $Zr_{44}Ti_{11}Cu_{10}Ni_{10}Be_{25}$ are supercooled liquid metals that soften on heating like thermoplastics suitable for FDM-based extrusion by heating to 460 °C [87]. The printing temperature T determines the incubation time t before recrystallisation according to the Arrhenius equation: $t = t_0 e^{-E/RT}$ where t_0 = time constant, E = activation energy, R = universal gas constant, T = annealing temperature. Deposition may proceed at a rate of 5 cm/s until the metallic glass recrystallises into hard metal within 100 s. Bulk metallic glass $La_{60}Ni_{15}Al_{25}$ has been suggested as a recyclable in-space material [88] but this is impractical. Furthermore, bulk metal glasses cannot be readily sourced and alloyed from lunar resources.

The most promising approach to 3D printing ceramics is peculiar to alumina through an inorganic ink for direct ink writing, comprising 58% alumina (Al_2O_3) particles ~80–200 nm within aluminium dihydrogen phosphate ($Al(H_2PO_4)_3$—AP) matrix as a rheological modifier [89]. AP may be synthesised by reacting H_3PO_4 with $Al(OH)_3$. The inorganic AP binder reduces shrinkage during sintering of the 3D printed alumina ceramic at 1250 °C for maximum bending strength. Additives reduce the sintering temperature from the Al_2O_3 sintering temperature of 1700–1800 °C. TheTiO_2 additive dissolves in Al_2O_3 while the CuO additive becomes liquid to fill pores. If the CuO additive can be omitted, this represents a highly suitable ink for use on the Moon that is not reliant on carbon polymers.

7. Lunar-Derived Clays

Here, we adopt clays as a ceramic material with plastic properties to avoid the use of polymers. Clays are hydrated aluminosilicates with ratios of SiO_2/Al_2O_3 of (2.0–5.0):1.0. Kaolinite clay ($2SiO_2 \cdot Al_2O_3 \cdot 2H_2O$) with a water-to-clay ratio of ~0.60 may be 3D printed by DIW through 1.0–1.6 mm diameter nozzles, cured at room temperature for 24 h and sintered at 1100–1200 °C for several hours to yield porcelain with a compressive strength of 20–50 MPa [90]. To prevent clogging of nozzles, clay may be enriched with additives; although sodium polyacrylate is a superior deflocculant to sodium silicate [65], the latter is incorporated into the lunar industrial ecology. The use of embedded temperature and relative humidity sensors for feedback yields strengths of 70 MPa for fired clay and 90 MPa for non-fired clay [91]. Layer-wise slurry deposition uses a slurry feedstock of regolith mixed with 40% hydrated montmorillonite clay, deposited via a blade in 25–100 µm layers [92]. During drying, water from the current layer is drawn into the substrate layer by capillary forces to create a dry high-density powder bed. Either binder jetting of polymer fluid or laser sintering of powder layer may be adopted. The completed 3D part is then sintered at 1130 °C in a furnace. Martian salts $MgSO_4$ binding with SiO_2 to form forsterite Mg_2SiO_4 or enstatite $Mg_2Si_2O_6$ could strengthen the part if Martian resources

were available. A lunar version could exploit Sorel cement as a binder at the cost of consuming Cl import from Earth reacting with lunar olivine:

$$3MgO + MgCl_2 + 11H_2O \rightarrow 3Mg(OH)_2 \cdot MgCl_2 \cdot 8H_2O$$

Bamboo fibre reinforcement may be added [93], a highly versatile material suited to a lunar agricultural facility [7].

Geopolymer is an alkali-activated cement such as the clay-like aluminosilicate metakaolin activated by sodium silicate (waterglass). They form a 3D network of covalent Si-O–Al bonds $M_n\{-(SiO_2)_z\text{-}AlO_2\} \cdot wH_2O$ where M = metal cation such as K^+ and Na^+, n = polymerisation degree, z = 1, 2 or 3, w = bound water. Geopolymer may be constructed from metakaolinite (dehydroxylated kaolinite) comprising 90–95% Al_2O_3 and SiO_2, which dissolves in an activating alkali such as NaOH or KOH. Plasticising fillers can alter the viscoelasticity. These are commonly organics such as sodium carboxymethyl starch which increases viscosity, but magnesium aluminium silicate is a smectite clay derived from feldspar that serves the same purpose. Geopolymer may be mixed with aggregates such as 20% silica sand, which reduces shrinkage. Three-Dimensional printing geopolymers may be via extrusion of geopolymer paste or geopolymer powders which are activated by NaOH solution, which gives a higher compression strength than KOH [94]. The Na_2CO_3 activation reaction proceeds more slowly, which may be desirable but requires a carbon source. Curing at high temperature ~100 °C increases mechanical strength. A lunar regolith simulant-based geopolymer ink, reinforced by carbon fibre/quartz in different patterns, forms a 3D printed composite to reduce the brittleness of the geopolymer; rectangular sandwich patterns yielded the highest compressive strengths of 20 MPa and 34 MPa in y and x directions [95]. Lunar-derived clays offer some of the promise of ceramics, but their true potential requires marriage with polymers.

8. Non-Clay Minerals and Their Uses

There are other uses for non-clay lunar minerals. On the Moon, olivine forsterite (Mg_2SiO_4) may be reacted with quartz (SiO_2) to form the orthopyroxene enstatite ($MgSiO_3$):

$$Mg_2SiO_4 + SiO_2 \rightarrow 2MgSiO_3$$

The hydration of enstatite yields serpentinite ($Mg_3Si_2O_5(OH)_4$) and talc ($Mg_3Si_4O_{10}(OH)_2$):

$$6MgSiO_3 + H_2O \rightarrow Mg_3Si_2O_5(OH)_4 + Mg_3Si_4O_{10}(OH)_2$$

Talc may be employed as a dry lubricant as an alternative to tungsten or molybdenum disulphide [96]. Exploitation of such lunar minerals as ceramic resources has yet to be explored.

9. Direct Solar Sintering/Melting

We consider, finally, direct thermal processing of ceramic materials including regolith. A layer of regolith around 2.5 m thick is required for a radiation shield to reduce exposed radiation to 5 REM. Crucial to the deployment of sintered regolith is compressive strength for load bearing. Implicit is the desirability of manufacturing equipment from lunar resources. Solar concentrators are mirrors or lenses that concentrate light according to the concentrator ratio given by [97]:

$$C = \frac{A_{conc}}{A_{spot}} = \frac{\varepsilon\sigma\left(T_{spot}^4 - T_{amb}^4\right)}{S_0\eta_{conc}}$$

where T_{spot} = spot temperature = 1800 °C to melt regolith, T_{amb} = ambient temperature (270 K) and η_{conc} = concentrator efficiency of 0.85 requiring C~400. Mirrors comprise an aluminium reflector with a cover of fused silica glass (derived from locally extracted SiO_2 or other transparent material such as $MgAl_2O_4$ spinel). Paraboloids may be approximated by multiple appropriately oriented flat mirrors but with some loss in performance. Fresnel lenses offer a higher concentration ratio than mirrors given by the following [97]:

$$C = \left(\frac{n}{n_{amb} sin\theta_{sun}} \right)^2$$

where n = 1.5 for glass, n = 1 for air, θ_{sun} = sun half-angle = 0.275° so C = 97,700 compared to a theoretical C = 45,900 for mirrors. Fresnel lenses comprise fused silica glass with a submicron structured surface constructed by transparent fused silica glass or spinel. Sintering increases regolith-effective thermal conductivity, allowing increased sintering depth by 45% [98]. Solar concentrators generate limited spot size resolution of >10 mm. Large-scale experiments with a 52 m^2 mirror reflecting onto a 147-mirror concentrator concentrated solar 800 W/m^2 onto 4 MW/m^2 [99]. Compressive strength of solar layer-sintered regolith is under 5 MPa which is considered marginal from the minimum required 3 MPa under lunar gravity. Compression strength was enhanced by a higher sintering temperature and shortening the cooling time between layers by reducing thermal stresses. Most experiments on sintered regolith simulants also use simulated solar sources (Xe lamps) to replicate atmosphere-less lunar lighting conditions. The Regolight project deployed solar sintering using Xe lamps concentrated by a parabolic mirror then oriented by a water-cooled flat mirror onto regolith simulant to sinter it layer-by-layer with 100 μm layers into 10 × 20 × 70 mm bricks. They 3D printed interlocking 3D printed tetrahedon bricks and flat dodecahedron tiles using layers ~2 mm thick but feature resolution was limited to >14 mm and compressive strength was poor at 2.5 MPa due to irregular delamination and warping [100–102]. In small-scale experiments using Xe lamps on small regolith samples, compressive strengths of solar sintered regolith can reach ~150 MPa [103]. Successful sintering of regolith simulant bricks with a compression strength of 45 MPa has been achieved through a two-stage process using a polyvinyl alcohol (PVA) binder [104]. The binder was pre-mixed with water, then mixed with regolith simulant and then cast into cubical blocks using a hydraulic press. The brick was then heated in a furnace at 600 °C to remove the binder, then at 1150 °C to sinter the regolith. The conclusion is that solar sintering of regolith is highly restrictive—it has a poor spot size resolution, yet it is limited to small-scale structures. Successful deployment for large-scale application requires the use of polymer binders even for bricks.

Our own preliminary experiments confirm these findings. We used two Fresnel lenses to experiment on the solar melting of LHS-1 highland lunar regolith simulant into glass (Figure 4).

Exolith LHS-1 lunar highland simulant comprises 74.4% anorthosite, 24.7% basalt, 0.4% ilmenite, 0.3% olivine and 0.2% pyroxene. The small/large Fresnel lens numerical aperture was 0.3/0.5 with a focal spot diameter of 8 mm/11 mm. Our experiments were conducted in August in Ottawa. We used the small lens to form melted lines and the large lens to form melted squares. In printing a line, the sun's azimuth movement caused the focus to spread, requiring periodic adjustment to maintain focus on a point for melting (Figure 5a). The first single layer print exhibited a melt depth of 4.37 mm after 3 min of concentrated solar exposure. The three-layer print was printed sequentially by brushing more regolith layers over melted regolith, then melting them, but the final surface was rougher than the underlying layers due to cloud interference (Figure 5b).

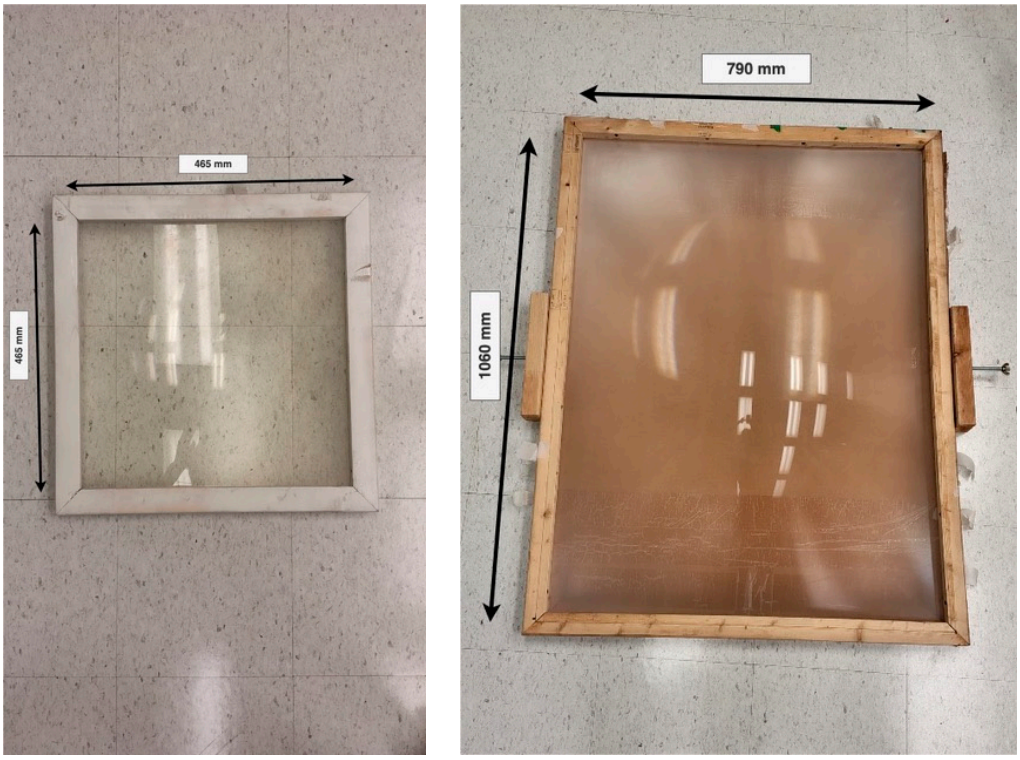

(**a**) (**b**)

Figure 4. (**a**) Small Fresnel lens; (**b**) Large Fresnel lens.

(**a**) (**b**)

Figure 5. (**a**) line of melted LHS-1; (**b**) square samples 1 to 4 of melted LHS-1.

The final square dimensions were 32.3 mm × 30.7 mm × 10.6 mm with each layer averaging ~3.5 mm (Figure 6).

All samples were compression load tested with squares of approximately the same dimensions on a substrate of unmelted regolith simulant (Figure 7).

Sample 1 was a three-layer sample, but the tests were performed on single-layered samples 2–4 to determine the compressive load limits (Table 1).

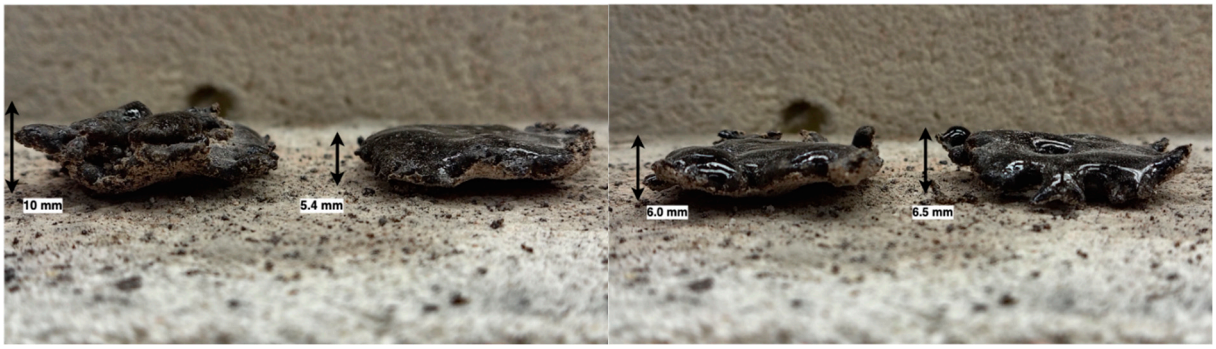

Figure 6. Thickness of samples 1 to 4 of melted LHS-1.

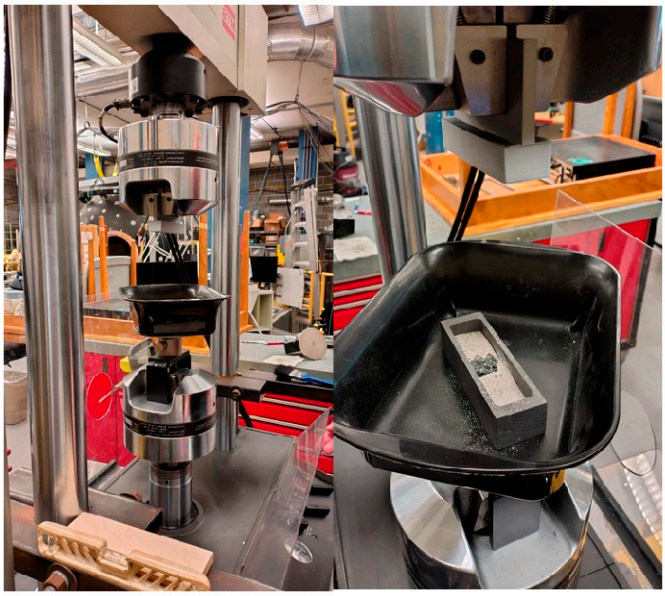

(**a**) (**b**)

Figure 7. (**a**) Compressive load testing apparatus; (**b**) sample under compression test.

Table 1. Melted sample compressive load limits until cracking.

Sample	Compressive Load Limit (N)
2	239
3	267
4	136 (crack 1)/446 (crack 2)—291 (av)

All the samples cracked into several pieces with a consistent compressive load of ~250 N (including offset tension of 24 N). With a probe cross-section of 110 mm × 29 mm, this gives a critical compressive pressure of 78 kPa, which is insufficient for adequate load bearing on the Moon.

10. Conclusions

The complexity of the ink of DIW and its reliance on polymers renders DIW unsuitable for the Moon even in support of human habitats; organic matter consumed in inks or binders must be either recycled through a closed loop capability or supplied from Earth. Although recycling may be plausible for some simple polymers, DIW inks are too complex to resynthesise. SLA-based methods similarly rely on photopolymers and photoinitiator polymers, but these are more plausibly manufacturable than DIW inks, though they still

require a carbon source. More traditional ceramic processing methods appear more suitable for lunar application. Sintering ceramics directly using solar concentrators is not reliant on the manufacture of organic polymers or other complex materials, though there remain issues regarding brittleness. Furthermore, to manufacture such optical devices from lunar resources reintroduces polymers. To exploit the full range and versatility of ceramics derived from lunar resources, carbon sources on the Moon to permit the synthesis of polymers must be searched for at the highest priority. Silicone polymers are preferred for deployment on the Moon for their hardiness to radiation. Although hydrocarbon polymers are susceptible to radiation effects, if used as a binder that is subsequently removed, this problem does not arise. The potential for lunar-derived ceramics is underexplored in comparison with lunar-derived metals. Lunar industrialisation will be critically dependent on the deployment of lunar ceramics, so this requires urgent address.

Funding: This research received no external funding.

Institutional Review Board Statement: Not applicable.

Informed Consent Statement: Not applicable.

Data Availability Statement: No new data were created or analysed in this study.

Acknowledgments: We would like to thank Aidan Chan for performing the solar Fresnel lens tests on the LHS-1 simulant.

Conflicts of Interest: The author declares no conflicts of interest.

References

1. Wang, Y.; Hao, L.; Li, Y.; Sun, Q.; Sun, M.; Huang, Y.; Li, Z.; Tang, D.; Wang, Y.; Xiao, L. In-situ utilisation of regolith resource and future exploration of additive manufacturing for lunar/martian habitats: A review. *Appl. Clay Sci.* **2022**, *229*, 106673. [CrossRef]
2. Mueller, R.; Howe, S.; Kochmann, D.; Ali, H.; Anderson, C.; Burgoyne, H.; Chambers, W.; Clinton, R.; De Kestellier, X.; Ebelt, K.; et al. Automated additive construction (AAC) for Earth and space using in-situ resources. In Proceedings of the Biennial ASCE Conference on Engineering, Science, Construction & Operations in Challenging Environments (Earth & Space 2016), Reston, VA, USA, 11–15 April 2016.
3. Fiske, M.; Ellery, A. *On the Development of an ISRU-Based Calcium Sulphoaluminate Concrete for 3D Printed and Cast Lunar Surface Infrastructure Applications*; AIAA SciTech Forum: Orlando, FL, USA, 2025; p. 1863.
4. Ellery, A. Leveraging in-situ resources for lunar base construction. *Can. J. Civ. Eng.* **2021**, *49*, 657–674. [CrossRef]
5. Ellery, A. Generating and storing power on the Moon using in-situ resources. *Proc. Inst. Mech. Eng. J. Aerosp. Eng.* **2021**, *236*, 1045–1063. [CrossRef]
6. Ellery, A. Can we build nuclear-electric propulsion systems from lunar resources? In *Space Resources Roundtable*; Colorado School of Mines: Golden, CO, USA, 2025; Available online: https://isruinfo.com/public/index.php?page=srr_25 (accessed on 12 August 2025).
7. Ellery, A. Supplementing closed ecological life support systems with in-situ resources on the Moon. *Life* **2021**, *11*, 770. [CrossRef]
8. Azami, M.; Kazemi, Z.; Moazen, S.; Dube, M.; Potvin, M.-J.; Skonieczny, K. Comprehensive review of lunar-based manufacturing and construction. *Prog. Aerosp. Sci.* **2024**, *150*, 101045. [CrossRef]
9. Zocca, A.; Wilbig, J.; Gunster, J.; Widjaja, P.; Neumann, C.; Clozel, M.; Meyer, A.; Ding, J.; Zhou, Z.; Tian, X. Challenges in the technology development for additive manufacturing in space. *Chin. J. Mech. Eng. Addit. Manuf. Front.* **2022**, *1*, 100018. [CrossRef]
10. Ellery, A. Challenges of robotic milli-g operations for asteroid mining. In Proceedings of the Future Technologies Conference 2024, London, UK, 14–15 November 2024; Arai, K., Ed.; Lecture Notes on Networks & Systems. Springer Nature Switzerland AG: Cham, Switzerland, 2024; Volume 1157, pp. 45–64.
11. McKay, D.; Hiken, G.; Basu, A.; Blanford, G.; Simon, S.; Reedy, R.; French, B.; Papike, J. Lunar regolith. In *Lunar Sourcebook*; Heiken, G., Vaniman, D., French, B., Eds.; Cambridge University Press: Cambridge, UK, 1991; pp. 287–356.
12. Klein, C. Lunar materials: Their mineralogy, petrology and chemistry. *Earth Sci. Rev.* **1972**, *8*, 169–204. [CrossRef]
13. Ellery, A. Sustainable in-situ resource utilisation on the Moon. *Planet. Space Sci.* **2020**, *184*, 104870. [CrossRef]
14. Sodha, G.; Dhingra, D. Novel geological framework to understand the origin and diversity of orthopyroxene, olivine, spinel (OOS) lithologies on the Moon. *Sci. Rep.* **2025**, *15*, 2426. [CrossRef]

15. Papike, J.; Taylor, L.; Simon, S. Lunar minerals. In *Lunar Sourcebook*; Heiken, G., Vaniman, D., French, B., Eds.; Cambridge University Press: Cambridge, UK, 1991; pp. 121–181.
16. Crawford, I.; Anand, M.; Barber, S.; Cowley, A.; Crites, S.; Fa, W.; Flahaut, J.; Gaddis, L.; Greenhagen, B.; Haruyama, J.; et al. Lunar resources. *Rev. Mineral. Geochem.* **2023**, *89*, 829–868. [CrossRef]
17. Reveron, H.; Gutierrez-Campos, D.; Rodriguez, R.; Bonassin, J. Chemical synthesis and thermal evolution of MgAl2O4 spinel precursor prepared from industrial gibbsite and magnesia powder. *Mater. Lett.* **2002**, *56*, 97–101. [CrossRef]
18. Ewais, E.; Besisa, D.; El-Amir, A.; El-Sheikh, S.; Rayan, D. Optical properties of nanocrystalline magnesium aluminate spinel synthesised from industrial waste. *J. Alloys Compd.* **2015**, *649*, 159–166. [CrossRef]
19. Lemeshev, D.; Senina, M.; Pedchenko, M.; Boyko, A. Transparent ceramic based on magnesium aluminate spinel for armour. *IOP Conf. Ser. Mater. Sci. Eng.* **2019**, *525*, 012081. [CrossRef]
20. Shi, Z.; Zhao, Q.; Guo, B.; Ji, T.; Wang, H. Review on processing polycrystalline magnesium aluminate spinel ($MgAl_2O_4$): Sintering techniques, material properties and machinability. *Mater. Des.* **2020**, *193*, 108858. [CrossRef]
21. Zhang, J.; Lu, T.; Chang, X.; Wei, N.; Qi, J. Unique mechanical properties of nanostructured transparent $MgAl_2O_4$ ceramics. *Nanoscale Res. Lett.* **2013**, *8*, 261. [CrossRef]
22. Mroz, T.; Goldman, L.; Gledhill, A.; Li, D.; Padture, N. Nanostructured infrared-transparent magnesium aluminate spinel with superior mechanical properties. *Int. J. Appl. Ceram. Technol.* **2012**, *9*, 83–90. [CrossRef]
23. Campos-Quiros, A.; Zughbi, M.; Kundu, A.; Watanabe, M. Correlation between grain boundary segregation behaviours of calcium and yttrium and enhanced fracture toughness in magnesium aluminate spinel. *J. Mater. Sci.* **2025**, *60*, 1826–1852. [CrossRef]
24. Voytovych, R.; MacLaren, I.; Gulgun, M.; Cannon, R.; Ruhle, M. Effect of yttrium on densification and grain growth in α-alumina. *Acta Mater.* **2002**, *50*, 3453–3463. [CrossRef]
25. Xu, P.; Wang, H.; Tu, B.; Gu, H.; Wang, W.; Liu, S.; Ma, C.; Fu, Z. Effect of yttrium-doped grain boundary on sintering behaviour and properties of transparent $ZnAl_2O_4$ ceramics. *J. Eur. Ceram. Soc.* **2024**, *44*, 6597–6606. [CrossRef]
26. Hou, Z.; Gong, Q.; Liu, N.; Jiang, B.; Li, J.; Wu, Y.; Huang, J.; Gu, W. Elemental abundances of Moon samples based on statistical distributions of analytical data. *Appl. Sci.* **2023**, *13*, 360. [CrossRef]
27. Heiken, G.; Vaniman, D.; French, B. *Lunar Sourcebook: A Users Guide to the Moon*; Cambridge University Press: Cambridge, UK, 1991; Available online: https://www.lpi.usra.edu/publications/books/lunar_sourcebook/pdf/LunarSourceBook.pdf (accessed on 12 August 2025).
28. Ellery, A. Mining asteroid versus mining the Moon—Can you have your cake and eat it? In *Space Resources Roundtable*; Colorado School of Mines: Golden, CO, USA, 2025.
29. Unterclass, M. Geomimetics and extreme biomimetics inspired by hydrothermal systems—What can we learn from nature for materials synthesis? *Biomimetics* **2017**, *2*, 8. [CrossRef]
30. Lasaga, A.; Soler, J.; Ganor, J.; Burch, T.; Nagy, K. Chemical weathering rate laws and global geochemical cycles. *Geochim. Cosmochim. Acta* **1994**, *58*, 2361–2386. [CrossRef]
31. Thibodeau, B.; Walls, X.; Ellery, A.; Cousens, B.; Marczenko, K. Extraction of silica and alumina from lunar highland simulant. In Proceedings of the ASCE Earth & Space Conference 2024, Miami, FL, USA, 15–18 April 2024; p. 6962.
32. Ellery, A.; Mellor, I.; Wanjara, P.; Conti, M. Metalysis FFC process as a strategic lunar in-situ resource utilisation technology. *New Space J.* **2022**, *10*, 224–238. [CrossRef]
33. Walls, X.; Ellery, A.; Marczenko, K.; Wanjara, P. Aluminium metal extraction from lunar highland simulant using electrochemistry. In Proceedings of the ASCE Earth & Space Conference 2024, Miami, FL, USA, 15–18 April 2024. Paper No. 7061.
34. Ellery, A. Is electronics fabrication feasible on the Moon? In Proceedings of the ASCE Earth & Space Conference 2022, Denver, CO, USA, 25–28 April 2022; pp. 759–772.
35. Dorcheh, S.; Abbasi, M. Silica aerogel: Synthesis, properties and characterization. *J. Mater. Process. Technol.* **2008**, *199*, 10–26. [CrossRef]
36. Hogue, M.; Mueller, R.; Sibille, L.; Hintze, P.; Rasky, D. Extraterrestrial regolith derived atmospheric entry heat shields. In Proceedings of the 15th Biennial ASCE International Conference on Engineering, Science, Construction, and Operations in Challenging Environments, Orlando, FL, USA, 11–15 April 2016.
37. Chen, Y.; Wang, X.; Yu, C.; Ding, J.; Deng, C.; Zhu, H. Properties of inorganic high temperature adhesive for high temperature furnace connection. *Ceram. Int.* **2019**, *45*, 8684–8689. [CrossRef]
38. McAdam, A.; Zolotiv, M.; Sharp, T.; Leshkin, L. Preferential low pH dissolution of pyroxene in plagioclase-pyroxene mixtures: Implications for martian surface materials. *Icarus* **2008**, *196*, 90–96. [CrossRef]
39. Baasch, J.; Windisch, L.; Koch, F.; Linke, S.; Stoll, E.; Schilde, C. Regolith as substitute mould material for aluminium casting on the Moon. *Acta Astronaut.* **2021**, *182*, 1–12. [CrossRef]
40. Marques, A.; Miglietta, D.; Gaspar, G.; Baptista, A.; Gaspar, A.; Perdigao, P.; Soares, I.; Bianchi, C.; Sousa, D.; Faustino, M.; et al. Synthesis of thermoelectric magnesium-silicide pastes for 3D printing, electrospinning and low-pressure spray. *Mater. Renew. Sustain. Energy* **2019**, *8*, 21. [CrossRef]

41. Frankberg, E. Ceramic that bends instead of shattering. *Science* **2022**, *378*, 359–360. [CrossRef]
42. Kuang, X.; Carotenuto, G.; Nicolais, L. Review of ceramic sintering and suggestions on reducing sintering temperatures. *Adv. Perform. Mater.* **1997**, *4*, 257–274. [CrossRef]
43. Vakifahmetoglu, C.; Karacasulu, L. Cold sintering of ceramics and glasses: A review. *Curr. Opin. Solid. State Mater. Sci.* **2020**, *24*, 100807. [CrossRef]
44. Yamasaki, N.; Yanagisawa, K.; Nishioka, M.; Kanahara, S. Hydrothermal hot-pressing method: Apparatus and application. *J. Mater. Sci. Lett.* **1986**, *5*, 355–356. [CrossRef]
45. Yanagisawa, K.; Nishioka, M.; Ioku, K.; Yamasaki, N. Densification of silica gels by hydrothermal hot-pressing. *J. Mater. Sci. Lett.* **1993**, *12*, 1073–1075. [CrossRef]
46. Chen, W.; Shui, A.; Wang, C.; Li, J.; Ma, J.; Tian, W.; Ota, T.; Xi, X. Preparation of aluminium titanate flexible ceramic by solid phase sintering and its mechanical behaviour. *J. Alloys Compd.* **2019**, *777*, 119–126. [CrossRef]
47. Kishimoto, A.; Obata, M.; Asaoka, H.; Hayashi, H. Fabrication of alumina-based ceramic foams utilising superplasticity. *J. Eur. Ceram. Soc.* **2007**, *27*, 41–45. [CrossRef]
48. Wakai, F.; Kondo, N.; Shinoda, Y. Ceramics superplasticity. *Curr. Opin. Solid. State Mater. Sci.* **1999**, *4*, 461–465. [CrossRef]
49. Pilling, J.; Payne, J. Superplasticity in Al2O3-ZrO2-Al2TiO5 ceramics. *Scr. Metall. Mater.* **1995**, *32*, 1091–1097. [CrossRef]
50. Shen, Z.; Peng, H.; Nygren, M. Formidable increase in the superplasticity of ceramics in the presence of an electric field. *Adv. Mater.* **2003**, *15*, 1006–1009. [CrossRef]
51. Dong, L.; Zhang, J.; Li, Z.; Gao, Y.; Wang, M.; Huang, M.; Wang, J.; Chen, K. Borrowed dislocations for ductility in ceramics. *Science* **2024**, *385*, 422–428. [CrossRef]
52. Peng, L.; Cao, J.; Noda, K.; Han, K. Mechanical properties of ceramic-metal composites by pressure infiltration of metal into porous ceramics. *Mater. Sci. Eng. A* **2004**, *374*, 1–9. [CrossRef]
53. Wan, F.; Zuo, Y.; Pan, Y.; Yu, A.; Qi, J.; Lu, X. Iron-enhanced simulated lunar regolith sintered blocks: Preparation, sintering and mechanical properties. *Constr. Build. Mater.* **2024**, *439*, 137395. [CrossRef]
54. Rahimian, M.; Ehsani, N.; Parvin, N.; Baharvandi, H. Effect of particle size, sintering temperature and sintering time on the properties of Al-Al_2O_3 composites made by powder metallurgy. *J. Mater. Process. Technol.* **2009**, *209*, 5387–5393. [CrossRef]
55. Azami, M.; Siahsarani, A.; Hadian, A.; Kazemi, Z.; Rahmatabadi, D.; Kashani-Bozorg, F.; Abrinia, K. Laser powder bed fusion of alumina/Fe-Ni ceramic matrix particulate composites impregnated with a polymeric resin. *J. Mater. Res. Technol.* **2023**, *24*, 3133–3144. [CrossRef]
56. Laot, M.; Rich, B.; Cheibas, I.; Fu, J.; Zhu, J.-N.; Popovich, V. Additive manufacturing and spark plasma sintering of lunar regolith for functionally graded materials. *Spool* **2021**, *8*, 7–23.
57. Faes, M.; Valkenaers, H.; Vogeler, F.; Vleugels, J.; Ferraris, E. Extrusion-based 3D printing of ceramic components. *Procedia CIRP* **2015**, *28*, 76–81. [CrossRef]
58. Ngo, T.; Kashani, A.; Imbalzano, G.; Nguyen, K.; Hui, D. Additive manufacturing (3D printing): A review of materials, methods, applications and challenges. *Compos. B Eng.* **2018**, *143*, 172–196. [CrossRef]
59. Fang, W.; Mu, Z.; He, Y.; Kong, K.; Jiang, K.; Tang, R.; Liu, Z. Organic-inorganic covalent-ionic molecules for elastic ceramic plastic. *Nature* **2023**, *619*, 293–299. [CrossRef]
60. Sun, S.; Mao, L.-B.; Lei, Z.; Yu, S.-H.; Colfen, H. Hydrogels from amorphous calcium carbonate and polyacrylic acid: Bio-inspired materials for 'mineral plastic'. *Angew. Chem. Int. Ed.* **2016**, *55*, 11765–11769. [CrossRef] [PubMed]
61. Wang, Y.; Wu, T.; Huang, G. State-of-the-art research progress and challenge of the printing techniques, potential applications for advanced ceramic materials 3D printing. *Mater. Today Commun.* **2024**, *40*, 110001. [CrossRef]
62. Clemens, F.; Sarraf, F.; Borzi, A.; Neels, A.; Hadian, A. Material extrusion additive manufacturing of advanced ceramics: Towards the production of large components. *J. Eur. Ceram. Soc.* **2023**, *43*, 2752–2760. [CrossRef]
63. Yeh, T.-S.; Sacks, M. Effect of particle size distribution on the sintering of alumina. *Commun. Am. Ceram. Soc.* **1988**, *71*, C484–C487. [CrossRef]
64. Wang, W.; Zhang, L.; Dong, X.; Wu, J.; Zhou, Q.; Li, S.; Shen, C.; Liu, W.; Wang, G.; He, R. Additive manufacturing of fibre reinforced ceramic matrix composites: Advances, challenges and prospects. *Ceram. Int.* **2021**, *48*, 19542–19556. [CrossRef]
65. Martin, J.; Fiore, B.; Erb, R. Designing bioinspired composite reinforcement architectures via 3D magnetic printing. *Nat. Commun.* **2015**, *6*, 8641. [CrossRef]
66. Romanczuk-Ruszuk, E.; Sztorch, B.; Pakula, D.; Gabriel, E.; Nowak, K.; Przekop, R. 3D printing ceramics—Materials for direct extrusion process. *Ceramics* **2023**, *6*, 364–385. [CrossRef]
67. Hao, L.; Tang, D.; Sun, T.; Xiong, W.; Feng, Z.; Evans, K.; Li, Y. Direct ink writing of mineral materials—A review. *Int. J. Precis. Eng. Manuf. Green. Technol.* **2021**, *8*, 665–685. [CrossRef]
68. Lamnini, S.; Elsaed, H.; Lakhdar, Y.; Baino, F.; Smeacetto, F.; Bernado, E. Robocasting of advanced ceramics: Ink optimization and protocol to predict the printing parameters—A review. *Helyon* **2022**, *8*, e10651. [CrossRef] [PubMed]

69. Chen, Z.; Li, Z.; Li, J.; Liu, C.; Lao, C.; Fu, Y.; Liu, C.; Li, Y.; Wang, P.; He, Y. 3D printing of ceramics: A review. *J. Eur. Ceram. Soc.* **2019**, *39*, 661–687. [CrossRef]
70. Shahzad, A.; Lazoglu, I. Direct ink writing of structural and functional ceramics: Recent achievements and future challenges. *Compos. B* **2021**, *225*, 109249. [CrossRef]
71. Jakus, A.; Koube, K.; Geisendorfer, N.; Shah, R. Robust and elastic lunar and martian structures from 3D printed regolith inks. *Sci. Rep.* **2017**, *7*, 44931. [CrossRef]
72. Rocha, V.; Saiz, E.; Tirichenko, I.; Garcia-Tunon, E. Direct ink writing advances in multi-material structures for a sustainable future. *J. Mater. Chem. A* **2020**, *8*, 15646–15657. [CrossRef]
73. Bland, P.; Cintala, M.; Horz, F.; Cressey, G. Survivability of meteorite projectiles—Results from impact experiments. In Proceedings of the 32nd Lunar & Planetary Science Conference, Houston, TX, USA, 12–16 March 2001; p. 1764.
74. Bland, P.; Artemieva, N.; Collins, G.; Bottke, W.; Bussey, D.; Joy, K. Asteroids on the Moon: Projectile survival during low velocity impacts. In Proceedings of the 39th Lunar & Planetary Science Conference, League City, TX, USA, 10–14 March 2008; p. 2045.
75. Halim, S.; Crawford, I.; Collins, G.; Joy, K.; Davison, T. Assessing the survival of carbonaceous chondrites impacting the lunar surface as a potential resource. *Planet. Space Sci.* **2024**, *246*, 105905. [CrossRef]
76. Joy, K.; Crawford, I.; Curran, N.; Zolensky, M.; Fagan, A.; King, D. Moon: An archive of small body migration in the solar system. *Earth Moon Planets* **2016**, *118*, 133–158. [CrossRef]
77. Yang, Y.; Li, S.; Zhu, M.-H.; Liu, Y.; Wu, B.; Du, J.; Fa, W.; Xu, R.; He, Z.; Wang, C.; et al. Impact remnants rich in carbonaceous chondrites detected on the Moon by the Chang'e 4 rover. *Nat. Astron.* **2022**, *6*, 207–213. [CrossRef]
78. Thomas-Keprta, K.; Clemett, S.; Messenger, S.; Ross, D.; Le, L.; Rahman, Z.; McKay, D.; Gibson, E.; Gonzalez, C.; Peabody, W. Organic matter on the Earth's Moon. *Geochim. Cosmochim. Acta* **2014**, *134*, 1–15. [CrossRef]
79. Ellery, A. Trials and tribulations of asteroid mining. In Proceedings of the ASCE Earth & Space Conference 2024, Miami, FL, USA, 15–18 April 2024; p. 8087.
80. O'Lenick, A. Basic silicone chemistry—A review. Silicone Spect. 2009. Available online: https://www.scientificspectator.com/documents/silicone%20spectator/Silicone_Spectator_January_2009.pdf (accessed on 12 August 2025).
81. Chaudhary, R.; Parameswaran, C.; Idrees, M.; Rasaki, A.; Liu, C.; Chen, Z.; Colombo, P. Additive manufacturing of polymer-derived ceramics: Materials, technologies, properties and potential applications. *Prog. Mater. Sci.* **2022**, *128*, 100969. [CrossRef]
82. Davis, P.; Murugavel, R. Recent developments in the chemistry of molecular titanosiloxanes and titanophosphonates. *Synth. React. Inorg. Met. Org. Nano-Met. Chem.* **2005**, *35*, 591–622. [CrossRef]
83. Unny, R.; Gopinathan, S.; Gopinathan, C. Chelated aluminosiloxanes. *Indian. J. Chem.* **1980**, *19A*, 484–486.
84. Puxviel, J.; Boilot, J.; Poncelet, O.; Hubert-Pfalzgraf, L.; Lecomte, A.; Dauger, A.; Beloeil, J. Aluminosiloxane as a ceramic precursor. *J. Non-Cryst. Solids* **1987**, *93*, 277–286. [CrossRef]
85. Griffith, M.; Halloran, J. Freeform fabrication of ceramics vis stereolithography. *J. Am. Ceram. Soc.* **1996**, *79*, 2601–2608. [CrossRef]
86. Dou, R.; Tang, W.; Hu, K.; Wang, L. Ceramic paste for space stereolithography 3D printing technology in microgravity environments. *J. Eur. Ceram. Soc.* **2022**, *42*, 3968–3975. [CrossRef]
87. Gibson, M.; Mykulowycz, N.; Shim, J.; Fontana, R.; Schmitt, P.; Roberts, A.; Ketkaew, J.; Shao, L.; Chen, W.; Bordeenithikasem, P.; et al. 3D printing metals like thermoplastics: Fused filament fabrication of metallic glasses. *Mater. Today* **2018**, *21*, 697–702. [CrossRef]
88. Liao, C.; Liu MZhang, Q.; Dong, W.; Zhao, R.; Li, B.; Jiao, Z.; Somg, J.; Yao, W.; Zhao, S.; Bai, H.; et al. Low temperature thermoplastic welding of metallic glass ribbons for in-space manufacturing. *Sci. China Mater.* **2020**, *64*, 979–986. [CrossRef]
89. Xu, X.; Zhang, J.; Jiang, P.; Liu, D.; Jia, X.; Wang, X.; Zhou, F. Direct ink writing of aluminium-phosphate-bonded Al_2O_3 ceramic with ultralow dimensional shrinkage. *Ceram. Int.* **2022**, *48*, 864–871. [CrossRef]
90. Revelo, C.; Colorado, H. 3D printing of kaolinite clay ceramics using direct ink writing (DIW) technique. *Ceram. Int.* **2018**, *44*, 5673–5682. [CrossRef]
91. Marquez, C.; Mata, J.; Renteria, A.; Gonzalez, D.; Gomez, G.; Lopez, A.; Baca, A.; Nunez, A.; Hassan, S.; Burke, V.; et al. Direct ink-write printing of ceramic clay with an embedded wireless temperature and relative humidity sensor. *Sensors* **2023**, *23*, 3352. [CrossRef] [PubMed]
92. Karl, D.; Kamutzki, F.; Lima, P.; Gili, A.; Duminy, T.; Zocca, A.; Gunster, J.; Gurlo, A. Sintering of ceramics for clay in situ resource utilisation of Mars. *Open Ceram.* **2020**, *3*, 100008. [CrossRef]
93. Tong, W.; Jaw, W.; Pothunuri, L.; Soh, E.; Le Ferrand, H. Easily applicable protocol to formulate inks for extrusion-based 3D printing. *Ceramica* **2022**, *68*, 152–159. [CrossRef]
94. Lazorenko, G.; Kasprzhitskii, A. Geopolymer additive manufacturing: A review. *Addit. Manuf.* **2022**, *55*, 102782. [CrossRef]
95. Ma, S.; Jiang, Z.; Fu, S.; He, P.; Sun, C.; Duan, X.; Jia, D.; Colombo, P.; Zhou, Y. 3D printed lunar regolith simulant-based geopolymer composites with bio-inspired sandwich architectures. *J. Adv. Ceram.* **2023**, *12*, 510–525. [CrossRef]
96. Abdulkareem, S.; Orkuma, G.; Apasi, A. Talc as a substitute for dry lubricant (an overview). *AIP Proc.* **2011**, *1315*, 1400.

97. *TM-2011-217114/AIAA-2011-704*; Thermal Energy for Lunar In Situ Resource Utilisation: Technical Challenges and Technology Opportunities. NASA: Washington, DC, USA, 2011.
98. Zhang, Y.; Shaw, M.; Brooks, G.; Rhamdhani, A.; Guo, C.; Han, Z.; Jackson, T.; Judkins, G. Investigation of heat transfer processes in multi-sized solar-sintered regolith for lunar ISRY program. *Int. J. Heat. Mass. Transf.* **2023**, *214*, 124387. [CrossRef]
99. Meurisse, A.; Makaya, A.; Willsch, C.; Sperl, M. Solar 3D printing of lunar regolith. *Acta Astronaut.* **2018**, *142*, 800–810. [CrossRef]
100. Imhof, B.; Urbina, D.; Weiss, P.; Sperl, M. Advancing solar sintering for building a base on the Moon. In Proceedings of the 67th International Astronautical Congress, Adelaide, Australia, 25–29 September 2017; IAC-17.C2.9.13.x37414.
101. Imhof, B.; Sperl, M.; Urbina, D.; Weiss, P.; Preisinger, C.; Waclavicek, R.; Hoheneder, W.; Meurisse, A.; Fateri, M.; Gobert, T.; et al. Using solar sintering to build infrastructure on the Moon: Latest advancements in the Regolight project. In Proceedings of the 69th International Astronautical Congress, Bremen, Germany, 1–5 October 2018; IAC-18.E5.1.x47746.
102. Fateri, M.; Meurisse, A.; Sperl, M.; Urbina, D.; Madakashira, K.; Govindaraj, S.; Gancet, J.; Imhof, B.; Hoheneder, W.; Waclavicek, R.; et al. Solar sintering for lunar additive manufacturing. *ASCE J. Aerosp. Eng.* **2019**, *32*, 04019101. [CrossRef]
103. Biswas, D.; Cox, T.; Lapp, J. Sintering behaviour of lunar soil heated by indirect and direct concentrated sunlight. In Proceedings of the ASME 16th International Conference on Energy, Philadelphia, PA, USA, 11–13 July 2022; Paper No. ESS2022-81630.
104. Gupta, N.; Dawara, V.; Kumar, A.; Viswanathan, K. Synthetic space bricks from lunar and martian regolith via sintering. *Adv. Space Res.* **2024**, *74*, 3902–3915. [CrossRef]